J. Mater. Chem. A

Supporting Information

Li^+-intercalated carbon cloth for anode-free Li-ion batteries with unprecedented cyclability

Amol Bhairuba Ikhe[a], Woon Bae Park[a,*], Su Cheol Han [a], Jung Yong Seo[a], Suyeon Han[a], Kee-Sun Sohn[b,*], Myoungho Pyo[a,*]

[a]*Department of Advanced Components and Materials Engineering, Sunchon national University, Chonnam 57922, Republic of Korea*

[b]*Faculty of Nanotechnology and Advanced Materials Engineering, Sejong University, Seoul 05006, Republic of Korea*

* Corresponding authors.

E-mail addresses: wbpark@scnu.ac.kr (W. B. Park), kssohn@sejong.ac.kr (K.-S. Sohn), mho@sunchon.ac.kr (M. Pyo)

Table S1. Summary on the strategies and performances for AFLIBs (LIBs only).

	Strategies	Full cell	Remark	Ref
Extra Li	Replenishable extra Li metal	Cu/Li ‖ LFP	Quite slow discharge to reactivate LFP by using extra Li	S1
	Li-rich $Li_2[Ni_{0.8}Co_{0.1}Mn_{0.1}]O_2$ cathode	Cu ‖ $Li_{1.37}$NMC811	Convert to NMC811 after 1st charge	S2
	Li_2O as a sacrificing agent on NMC811	Cu ‖ Li_2O/NMC811	Convert to $Li_{2-x}O$ after releasing extra Li^+ during 1st charge	S3
Surface modified Cu	CVD-grown graphene	Cu/graphene ‖ LFP	61% Q retention after 100 cycles	S4
	Al_2O_3/polyacrylonitrile composite layer	Cu/AOP ‖ NMC111	30% Q retention for 82 cycles	S5
	Spin-coated GO	Cu/GO ‖ NMC111	44% Q retention for 50 cycles	S6
	PEO	Cu/PEO ‖ LFP	30% Q retention after 200 cycles	S7
	Ag@PDA/GO	Cu/Ag@PDA/GO ‖ NMC111	55.7% Q retention after 60 cycles	S8
	Garnet:PVdF:$LiClO_4$	Cu/Garnet/PVdF/$LiClO_4$ ‖ NMC111	59% Q retention after 30 cycles	S9
	Spin coated LLZTO/PEO-CPE	Cu ‖ LLZTO/PEO-CPE ‖ NMC	41.2% Q retention after 65 cycles at 55 °C	S10
	Sn primer layer	Cu/Sn ‖ NCA	Convert to Sn-Li alloy during initial plating, then Li P/S cycles on Sn-Li	S11
	Benzotriazole coated Cu	BTA-Cu ‖ LFP	73% Q retention after 50 cycles	S12
	β-PVDF on Cu with thermal-electrochemical activation	Cu/β-PVDF‖ NMC111	61.4% Q retention after 30 cycles	S13
	Ag@P-APF	Cu/Ag@P-APF ‖ NMC	40% Q retention after 70 cycles	S14
	LiF@PVDF dielectric layer	Cu/LiF@PVDF ‖ LFP	<60% Q retention after 40 cycles	S15
	Laser-induced SiOx layer	Cu/LI-SiOx ‖ LFP	45.6% Q retention after 100 cycles	S16
	Dielectric blocks of $BaTiO_3$ on Cu	Cu/BTO ‖ NMC	~83% Q retention after 50 cycles	S17
	Ultrathin Zn-NC-CNT interfacial layer on Cu	Cu/Zn-NC-CNT ‖ NMC811	~85% Q retention after 50 cycles	S18
Electro-lyte	4M LiFSI in DME	Cu ‖ LFP	54% Q retention after 100 cycles	S19
	1M $LiPF_6$ in FEC/TTE/EMC	Cu ‖ NMC111	40% Q retention for 80 cycles	S20
	Mixed salt (2M LiFSI + 1M LiTFSI) in DME/DOL	Cu ‖ LFP	50% Q retention after 50 cycles	S21
	2M $LiPF_6$ in EC/DEC/FEC	Cu ‖ NMC111	40% Q retention for 50 cycles	S22
	3M LiFSI in DOL/DME, plating & then 24h resting	Cu ‖ LFP	64% Q retention after 50 cycles	S23
	2 wt% KPF_6 & 2 vol% TMSP in 1M $LiPF_6$/EC:DEC	Cu ‖ NMC111	48% Q retention after 20 cycles	S24
	KNO_3 additive in 1M $LiPF_6$/EC:DMC	Cu ‖ NMC111	40% Q retention after 50 cycles	S25
	1M LiDFOB+0.05M $LiPF_6$ in FEC:TTE:DEC	Cu ‖ NMC532	45% Q retention after 35 cycles	S26
	1M $LiPF_6$ in FEC:TTE (3:7)	Cu ‖ NMC111	50% Q retention after 65 cycles	S27
	2M LiFSI+2M$LiNO_3$ in DME	Cu ‖ NMC	47.3% Q retention after 100 cycles	S28
		Cu ‖ LFP	52.7% Q retention after 100	

			cycles	
	1M LiTFSI in TMS+FEC(8:2)	Cu ‖ NMC811	<30% Q retention after 25 cycles	S29
	0.2M $LiPF_6$+3.8M LiTFSI +0.2wt% $LiNO_3$ in EC/DEC/EMC/TEP (1.5:2.5:1:5)	Cu ‖ LFP	54.8% Q retention after 50 cycles	S30
	4.6M LiFSI+2.3M LiTFSI in DME	Cu ‖ NMC622	~55% Q retention after 25 cycles	S31
	VEC additive in 1M $LiPF_6$ in EC/DMC	Cu ‖ NMC811	<15% Q retention after 50 cycles	S32
	1.5M $LiPF_6$+1wt% TMSB in FEC/EMC/DMC (34.6:57.2:8.2)	Cu ‖ NMC811	<20% Q retention after 30 cycles	S33
	1M $LiPF_6$ in EA/FEC/TTE/EMC (2:1:5:2)	Cu ‖ NMC111	<25% Q retention after 60 cycles	S34
	1M LiFSI in Fluorinated 1,4-dimethoxylbutane	Cu ‖ NMC	80% Q retention after 100 cycles	S35
	Triethylmethylphosphonium bis(fluorosulfonyl)imide [P_{1222}] [FSI] (Boron Molecular) ionic liquid and LiFSI (1:1 mol ratio)	Cu ‖ LFP	47.3% Q retention after 100 cycles	S36
		Cu ‖ sc-NMC622	53% Q retention after 100 cycles	
P & Temp control	1M $LiPF_6$ in FEC:TFEC under 1200 kPa	Cu ‖ NMC111		S37
	0.6M LiDFOB:0.6M $LiBF_4$/FEC:DEC under pressure	Cu ‖ NMC111	80% Q retention after 90 cycles	S38
	Hot-formation with pressure	Cu ‖ NMC532	80% Q retention after 195 cycles	S39
Other substrates	Defective carbon layer coated carbon paper	d-CP ‖ NMC811	56% Q retention after 100 cycles	S40
	Mesoporous silica thin film on the stainless steel foil	SS/MSTF ‖ LFP	~45% Q retention after 100 cycles	S41

References

S1 H. Liu, J. Holoubek, H. Zhou, Z. Wu, X. Xing, S. Yu, G. M. Veith, Y. Li, Y. Choi and P. Liu, *Energy Storage Mater*. 2021, **36**, 251-256.

S2 L. Lin, K. Qin, Q. Zhang, L. Gu, L. Suo, Y.-S. Hu, H. Li, X. Huang and L. Chen, *Angew*. *Chem*. *Int*. *Ed*. 2021, **60**, 8289-8296.

S3 Y. Qiao, H. Yang, Z. Chang, H. Deng, X. Li and H. Zhou, *Nat*. *Energy* 2021, **6**, 653-662.

S4 A. A. Assegie, C.-C. Chung, M.-C. Tsai, W.-N. Su, C.-W. Chen and B.-J. Hwang, *Nanoscale* 2019, **11**, 2710-2720.

S5 A. A. Sahalie, Z. T. Wondimkun, W.-N. Su, M. A. Weret, F. W. Fenta, G. B. Berhe, C.-J. Huang, Y.-C. Hsu and B. J. Hwang, *ACS Appl*. *Energy Mater*. 2020, **3**, 7666-7679.

S6 Z. T. Wondimkun, T. T. Beyene, M. A. Weret, N. A. Shahilie, C.-J. Huang, B. Thirmalaraj, B. A. Jote, D. Wang, W.-N. Su, C.-H. Wang, G. Brunklaus, M. Winter and B.-J. Hwang, *J*. *Power Sources* 2020, **450**, 227589.

S7 A. A. Assegie, J.-H. Cheng, L.-M. Kuo, W.-N. Su and B.-J. Hwang, *Nanoscale* 2018, **10**, 6125-6138.

S8 Z. T. Wondimkun, W. A. Tegegne, J. S.-Kai, C.-J. Huang, N. A. Sahilie, M. A. Weret, J.-Y. Hsu, P.-L. Hsieh, Y.-S. Huang, S.-H. Wu, W.-N. Su and B. J. Hwang, *Energy Storage Mater*. 2021, **35**, 334-344.

S9 L. H. Abrha, T. A. Zegeye, T. T. Hagos, H. Sutiono, T. M. Hagos, G. B. Berhe, C.-J. Huang, S.-K. Jiang, W.-N. Su, Y.-W. Yang and B.-J. Hwang, *Electrochim*. *Acta* 2019, **325**, 134825.

S10 T. A. Zegeye, W.-N. Su, F. W. Fenta, T. S. Zeleke, S.-K. Jiang and B. J. Hwang, *Energy Mater*. 2020, **3**, 11713-11723.

S11 S. S. Zhang, X. Fan and C. Wang, *Electrochim*. *Acta* 2017, **258**, 1201-1207.

S12 T. Kang, J. Zhao, F. Guo, L. Zheng, Y. Mao, C. Wang, Y. Zhao, J. Zhu, Y. Qiu, Y. Shen and L. Chen, *ACS Appl*. *Mater*. *Interfaces* 2020, **12**, 8168-8175.

S13 L. H. Abrha, Y. Nikodimos, H. H. Weldeyohannes, T. T. Hagos, D.-Y. Wang, C.-J. Huang, S.-K. Jiang, S.-H. Wu, W.-N. Su, M.-C. Tsai and B. J. Hwang, *ACS Appl*. *Mater*. *Interfaces* 2021, **4**, 3240-3248.

S14 N. T. Temesgen, W. A. Tegegne, K. N. Shitaw, F. W. Fenta, Y. Nikodimos, B. W. Taklu, S.-K. Jiang, C.-J. Huang, S.-H. Wu, W.-N. Su and B.-J. Hwang, *J*. *Taiwan Inst*. *Chem*. *Eng*. 2021, **128**, 87-97.

S15 O. Tamwattana, H. Park, J. Kim, I. Hwang, G. Yoon, T.-H. Hwang, Y.-S. Kang, J. Park, N. Meethong and K. Kang, *ACS Energy Lett*. 2021, **6**, 4416-4425.

S16 W. Chen, R. V. Salvatierra, M. Ren, J. Chen, M. G. Stanford and J. M. Tour, *Adv*. *Mater*. 2020, **31**, 2002850.

S17 C. Wang, M. Liu, M. Thijs, F. G. B. Ooms, S. Ganapathy and M. Wagemaker, *Nat*. *Commun*. 2021, **12**, 6536.

S18 T. Zhao, S. Li, Y. Wang, H. Wang, M. Zhang, X. Tang, F. Liu, D. Du, H. Zheng and Y. Ma, *J*. *Mater*. *Chem*. *A* 2021, **9**, 21281-21290.

S19 J. Qian, B. D. Adams, J. Zheng, W. Xu, W. A. Henderson, J. Wang, M. E. Bowden, S. Xu, J. Hu and J.-G. Zhang, *Adv*. *Funct*. *Mater*. 2016, **26**, 7094-7102.

S20 T. M. Hagos, T. T. Hagos, H. K. Bazabh, G. B. Berhe, L. H. Abrha, S.-F. Chiu, C.-J. Huang, W.-N. Su and H. Dai, *ACS Appl*. *Energy Mater*. 2020, **3**, 10722-10733.

S21 T. T. Beyene, H. K. Bezabh, M. A. Weret, T. M. Hagos, C.-J. Huang, C.-H. Wang, W.-N. Su, H. Dai and B.-J. Hwang, *J*. *Electrochem*. *Soc*. 2019, **166**, A1501-A1509.

S22 T. M. Hagos, B. Thirumalraj, C.-J. Huang, L. H. Abrha, T. M. Hagos, G. B. Berhe, H. K. Bezabh, J. Cherng, S.-F. Chiu, W.-N. Su and B.-J. Hwang, *ACS Appl*. *Energy Mater*. 2019, **11**, 9955-9963.

S23 T. T. Beyene, B. A. Jote, Z. T. Wondimkun, B. W. Olbassa, C.-J. Huang, B. Thirumalraj, C.-H. Wang, W.-N. Su, H. Dai and B.-J. Hwang, *ACS Appl*. *Energy Mater*. 2019, **11**, 31962-31971.

S24 T. M. Hagos, G. B. Berhe, T. T. Hagos, H. K. Bezabh, L. H. Abrha, T. T. Beyene, C.-J. Huang, Y.-W. Yang, W.-N. Su, H. Dai and B.-J. Hwang, *Electrochim*. *Acta* 2019, **316**, 52-59.

S25 N. A. Sahalie, A. A. Assegie, W.-N. Su, Z. T. Wondimkun, B. A. Jote, B. Thirumalraj, C.-J. Huang, Y.-W. Yang and B.-J. Hwang, *J*. *Power Sources* 2019, **437**, 226912.

S26 B. A. Jote, T. T. Beyene, N. A. Sahalie, M. A. Weret, B. W. Olbassa, Z. T. Wondimkun, G. B. Berhe, C.-J. Huang, W.-N. Su and B. J. Hwang, *J*. *Power Sources* 2020, **461**, 228102.

S27 T. T. Hagos, W.-N. Su, C.-J. Huang, B. Thirumalraj, S.-F. Chiu, L. H. Abrha, T. M. Hagos, H. K. Bezabh, G. B. Berhe, W. A. Tegegne, J.-Y. Cherng, Y.-W. Yang and B.-J. Hwang, *J*. *Power Sources* 2020, **461**, 228053.

S28 D. W. Kang, J. Moon, H.-Y. Choi, H.-C. Shin and B. G. Kim, *J*. *Power Sources* 2021, **490**, 229504.

S29 L. Dong, Y. Liu, D. Chen, Y. Han, Y. Ji, J. Liu, B. Yuan, Y. Dong, Q. Li, S. Zhou, S. Zhong, Y. Liang, M. Yang, C. Yang and W. He, *Energy Storage Mater*. 2022, **44**, 527-536.

S30 H. Choi, Y. Bae, S.-M. lee, Y.-C. Ha, H.-C. Shin and B. G. Kim, *J*. *Electrochem*. *Sci*. *Technol*. 2022, **13**, 78-89.

S31 J. Alvarado, M. A. Schroeder, T. P. Pollard, X. Wang, J. Z. Lee, M. Zhang, T. Wynn, M. Ding, O. Borodin, Y. S. Meng and K. Xu, *Energy Environ*. *Sci*. 2019, **12**, 780-794.

S32 S. Fang, Y. Zhang and X. Liu, *Chem*. *Eng*. *J*. 2021, **426**, 121880.

S33 K. Huang, S. Bi, B. Kurt, C. Xu, L. Wu, Z. Li, G. Feng and X. Zhang, *Angew*. *Chem*. *Int*. *Ed*. 2021, **60**, 19232-19240.

S34 T. M. Hagos, H. K. Bezabh, H. G. Redda, E. A. Moges, W.-H. Huang, C.-J. Huang, W.-N. Su, H. Dai and B. J. Hwang, *J*. *Power Sources* 2021, **512**, 220388.

S35 Z. Yu, H. Wang, X. Kong, W. Huang, Y. Tsao, D. G. Mackanic, K. Wang, X. Wang, W. Huang, S. Choudhury, Y. Zheng, C. V. Amanchukwu, S. T. Hung, Y. Ma, E. G. Lomeli, J. Qin, Y. Cui and Z. Bao, *Nat*. *Energy* 2020, **5**, 526-533.

S36 T. Pathirana, R. Kerr, M. Forsyth and P. C. Howlett, *Sustain*. *Energy Fuels* 2021, **5**, 4141-4152.

S37 A. J. Louli, M. Genovese, R. Weber, S. G. Hames, E. R. Logan and J. R. Dahn, *J. Electrochem. Soc*. 2019, **166**, A1291-A1299.

S38 R. Weber, M. Genovese, S. Hames, C. Martin, I. G. Hill and J. R. Dahn, *Nat. Energy* 2019, **4**, 683-689.

S39 M. Genovese, A. J. Louli, R. Weber, C. Martin, T. Taskovic and J. R. Dahn, *J. Electrochem. Soc*. 2019, **166**, A3342-A3347.

S40 H. Kwon, J.-H. Lee, Y. Roh, J. Baek, D. J. Shin, J. K. Yoon, H. J. Ha, J. Y. Kim and H.-T. Kim, *Nat. Commun*. 2021, **12**, 5537.

S41 C.-A. Lo, C.-C. Chang, Y.-W. Tsai, S.-K. Jiang, B. J. Hwang, C.-Y. Mou and H.-L. Wu, *ACS Appl. Energy Mater*. 2021, **4**, 5132-5142.

Table S2. List of abbreviations used in the manuscripts (excluding commonly used abbreviations. e.g. nm, µm, etc.)

Abbreviations	Full name
AFLIBs	Anode-free Li-ion batteries
CC	Carbon cloth
CP	Carbon paper
CF	Carbon foil
C/D	Charge/discharge
ED	Energy density
LIBs	Li-ion batteries
LMBs	Li-metal batteries
SEI	Solid-electrolyte-interface
P/S	Plating/stripping
wt%	Weight percentage
$LiPF_6$	Lithium hexafluorophosphate
EC/DMC	Ethylene carbonate/dimethyl carbonate
TEMPO	2,2,6,6-tetramethylpiperidine-1-oxyl
LFP	$LiFePO_4$
FESEM	Field emission scanning electron microscopy
EDX	Energy dispersive X-ray spectroscopy
AFM	Atomic force microscopy
FETEM	Field-emission transmission electron microscopy
SEI/CC^O	SEI formed CC in the oxidized state
SEI/CC^R	SEI formed CC in the reduced state
XRD	X-ray diffraction
XPS	X-ray photoelectron spectroscopy
EIS	Electrochemical impedance spectra
OCV	Open circuit voltage
CVs	Cyclic voltammograms
RMS	Root mean square
CE	Coulombic efficiency
LED	Light Emitting diodes

Comparison of carbon substrates used for this study

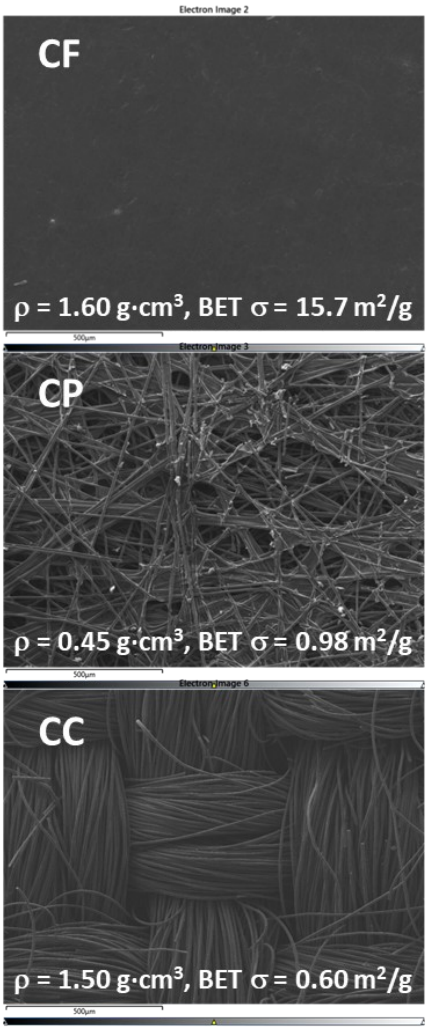

Fig. S1 FESEM images for CF, CP, and CC. Density (ρ) is from the manufacturers and BET σ (Brunauer, Emmett, and Teller surface area) was calculated from N_2 adsorption (Belsorp-max, MicrotracBEL, Corp.).

CF is a compressed graphite sheet with a thickness of 220 μm, obtained from Samjungcng, Korea (samjungcng.co.kr). It is made by homogeneously compressing the natural graphite flakes.

CP with a thickness of 190 μm (Toray TGP-H-120) was purchased from FuelCellsEtc. CP is made of irregularly interwoven carbon fibers (polyacrylonitrile-based), which are firmly connected by carbon films.

Plain CC with a thickness of 356 μm (1071) was purchased from FuelCellsEtc. CC1071 has an interwoven structure, and usual paper production techniques are used for manufacture.

Prior to use, all electrodes were cleaned by brief flame-burning (ca. 10 s).

FESEM images show that, while CF has no characteristic surface features, CC has an aligned carbon fibers (10 μm in diameter). CP is composed of randomly oriented carbon fibers (ca. 10 μm in diameter) integrated with graphitic binders.

Determination of electrochemically active surface areas of CF, CP, and CC

Electrochemically active areas were determined from cyclic voltammograms of TEMPO (2,2,6,6-tetramethylpiperidine-1-oxyl, 20 mM) in 1.0 M $LiPF_6$/EC:DMC. **Fig. S2** shows quasi-reversible voltammograms of TEMPO at 0.5 $mV \cdot s^{-1}$. The Randles-Sevcik equation was applied to calculate the electrode area. The anodic peak current and the diffusion coefficient of 9.2 x 10^{-6} $cm^2 \cdot s^{-1}$ (*Energy Adv.* 2022, **1**, 21.) were adopted. The smallest area of 1.04 cm^2 was obtained for CC, relative to 1.69 and 1.50 cm^2 for CF and CP, respectively, in CR2032 coin-type cells.

Note that, though CC has a cylindrical shape, the Randles-Sevcik equation, which is based on the linear diffusion, can be applied for the determination of an electrode area. The radial diffusion becomes important either when the length of cylinder is short compared to the radius (*Phys. Chem. Chem. Phys*. 2018, **20**, 148.) or when the scan rate is slow (*J. Electroanal. Chem*. 2020, **859**, 113865.), both of which are not the case in this study.

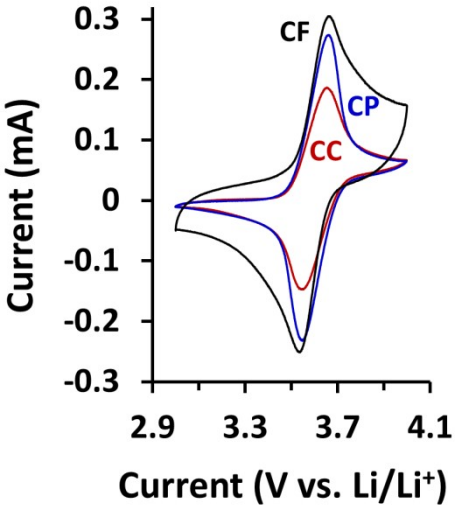

Fig. S2 Cyclic voltammograms of TEMPO on CF, CP, and CC in coin-type cells. The electrochemically active areas of 1.69, 1.50, and 1.04 cm^2 for CF, CP, and CC, respectively, were obtained.

Marginal changes in SEI compositions on CC

In contrast to a gradual increase in oxygen and fluorine contents of SEI on CF and CP, the SEI compositions on CC are almost invariant with cycling (0.02 - 3.0 V, 20 mA·g^{-1}) once formed during the 1st cathodic scan (^{1}R). For example, the fluorine and oxygen contents slightly increase after the 1st anodic scan (from ^{1}R to ^{1}O), but the change is negligible considering an error range in EDX. The compositional variation is also marginal after 5 and 10 cycles irrespective of the redox states, which signifies the irreversible formation of the robust SEI on the CC after the 1st cathodic scan (^{1}R).

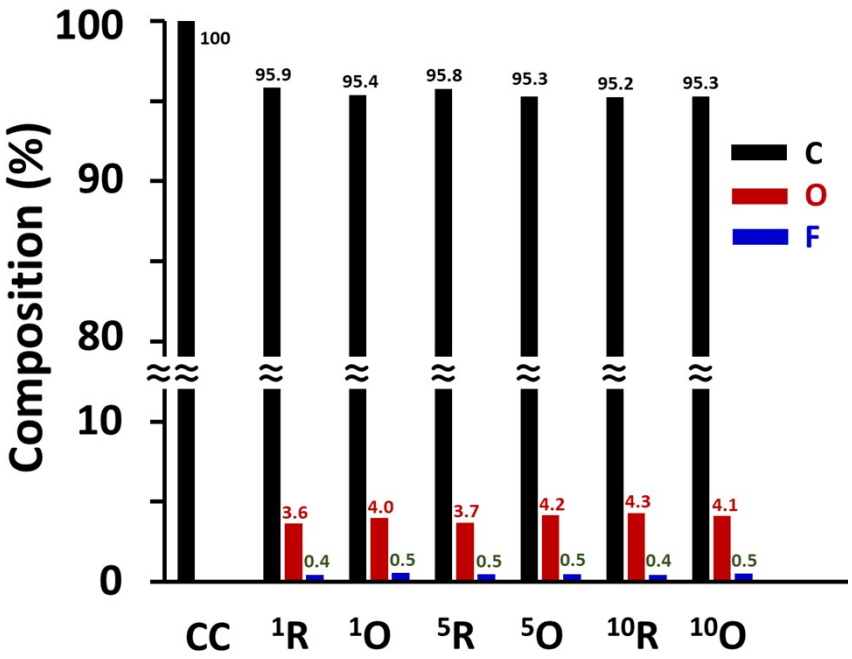

Fig. S3 Variation of elemental compositions examined using EDX. Superscript numerals on the abscissa indicate the number of galvanostatic cycles in a cell of CC ‖ Li, and R and O denote the reduced state at 0.02 V and the oxidized state at 3.0 V, respectively.

EDX spectra of SEI-formed CF and CP with cycles

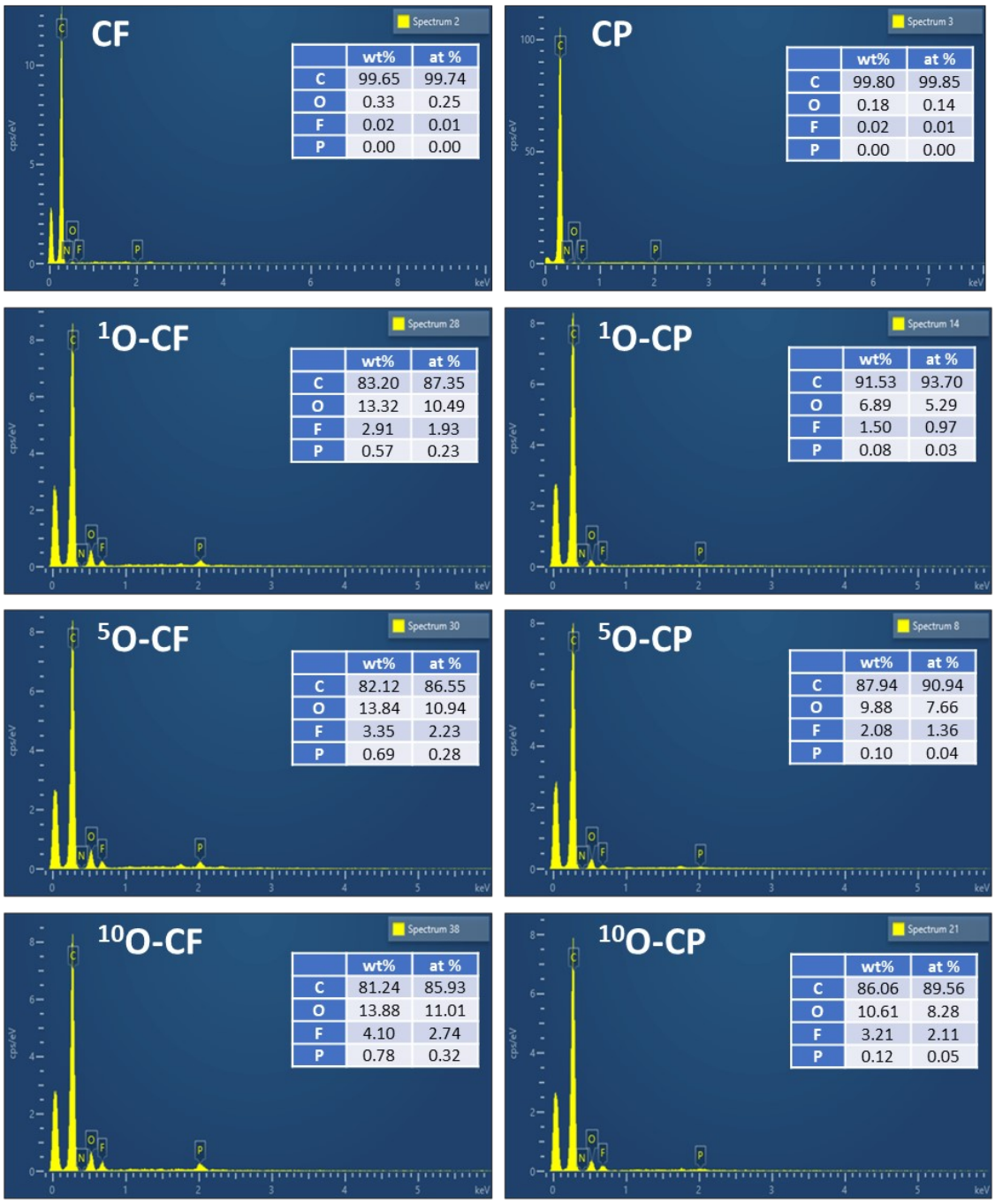

Fig. S4 EDX spectra of CF and CP electrodes subjected to galvanostatic cycles in coin-type cells between 0.02 and 3.0 V. Superscript numerals indicate the number of cycles, and O denotes the oxidized state at 3.0 V.

EDX spectra of SEI/CC^{R} and SEI/CC^{O} with cycles

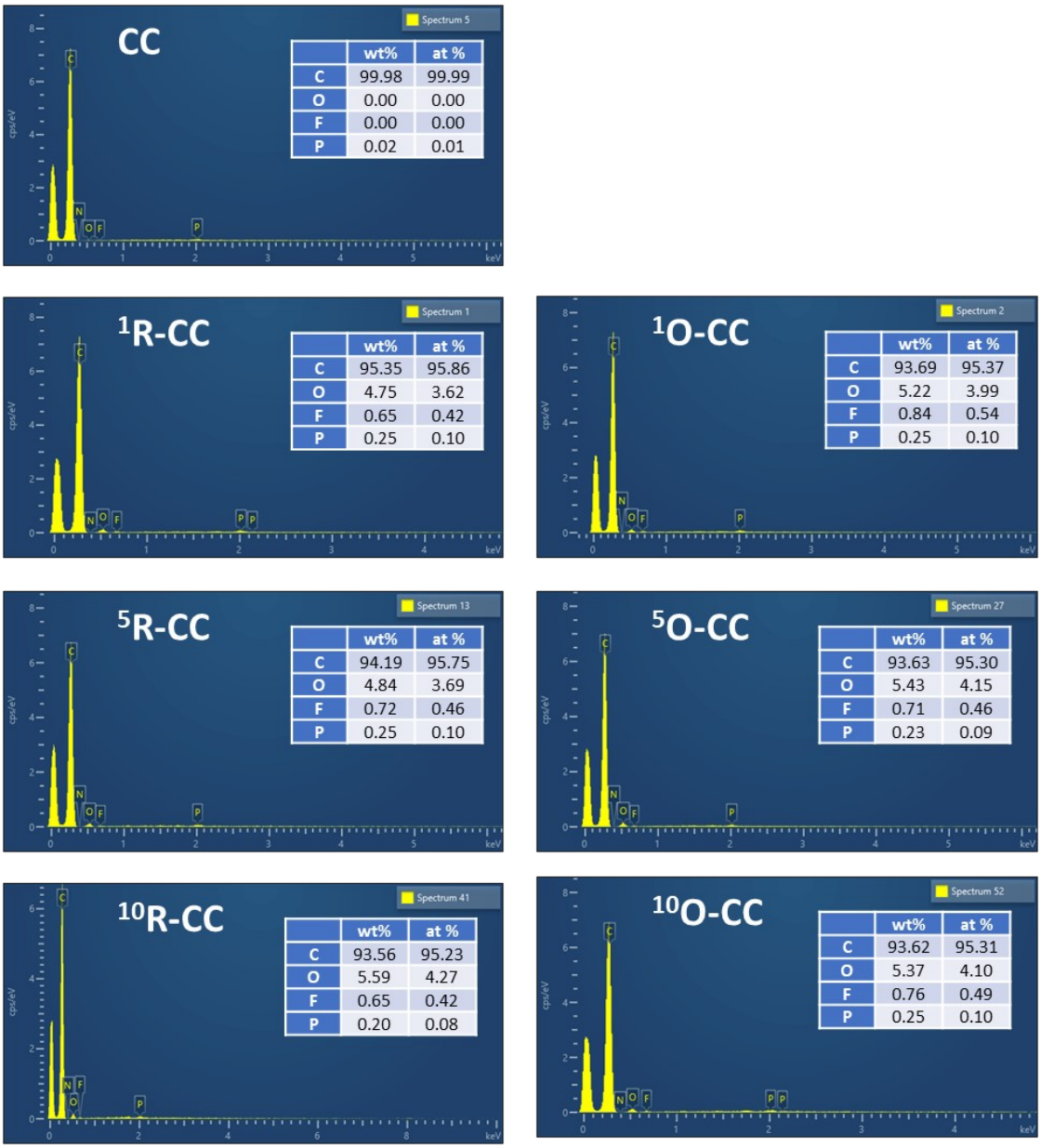

Fig. S5 EDX spectra of CC electrodes subjected to galvanostatic cycles in coin-type cells between 0.02 and 3.0 V. Superscript numerals indicate the number of cycles, and R and O denote the reduced state at 0.02 V and the oxidized state at 3.0 V, respectively.

FETEM image also supports that SEI is immediately formed on CC

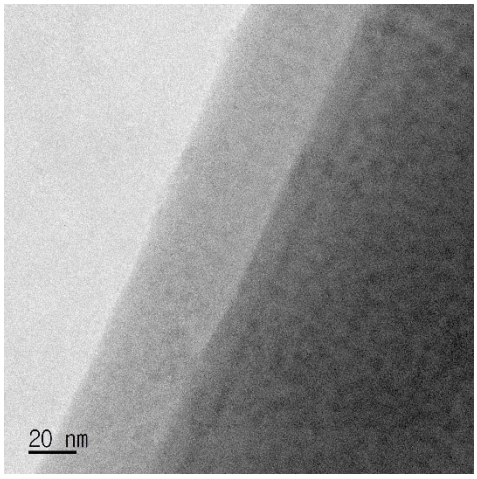

Fig. S6 FETEM image of SEI/CC^{R} after a single scan to 0.02 V. The thickness and uniformity of SEI are identical to that in Figure 2B, indicating that the SEI formation on CC is complete after a single cathodic scan to 0.02 V.

FESEM image of stripped CC reveals the perfect reversibility for Li P/S

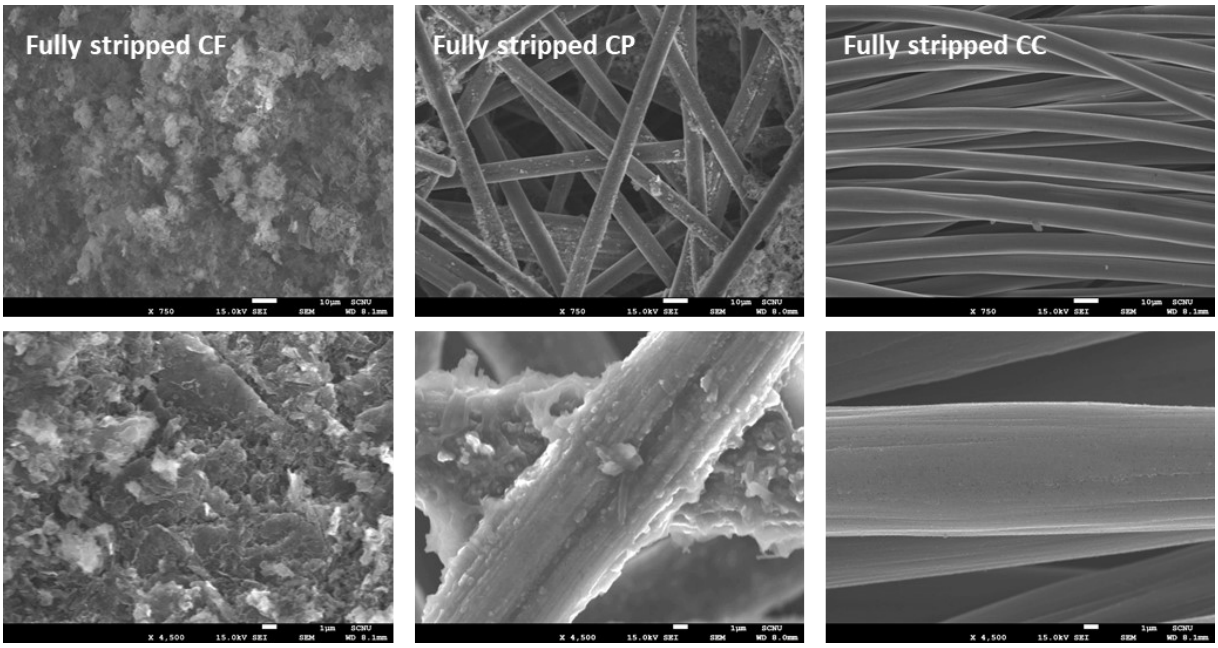

Fig. S7 FESEM images of fully stripped CF, CP, and CC. In contrast to CF and CP, CC shows no Li remaining, indicating the perfect reversibility for Li P/S processes.

Negligible Li^+ intercalation at voltages lower than 0.02 V

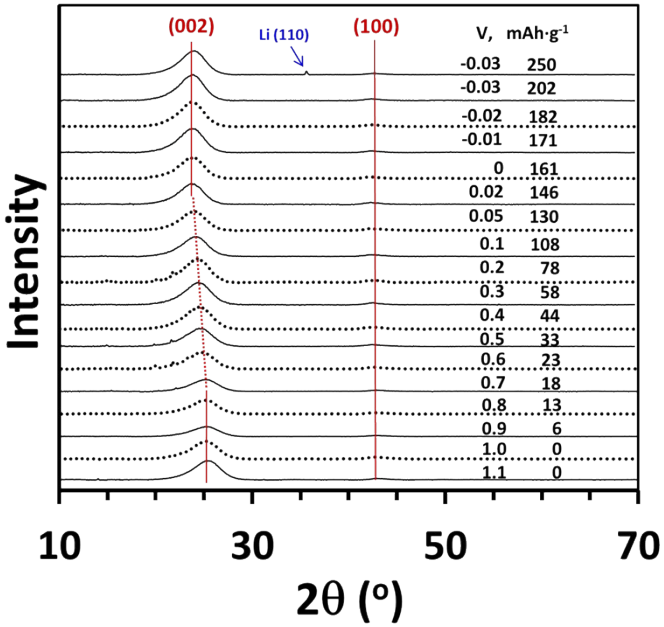

Fig. S8 Evolution of XRD patterns of CC during a scan toward the negative voltages. It is obvious that the d_{002} peaks move toward lower 2θ angles with Li^+ intercalation, but become stationary from the voltage lower than 0.02 V, which implies that no more Li^+ ions are intercalated into SEI/CC^R.

XPS reveals continuous increase of oxygen functionalities with ozone irradiation

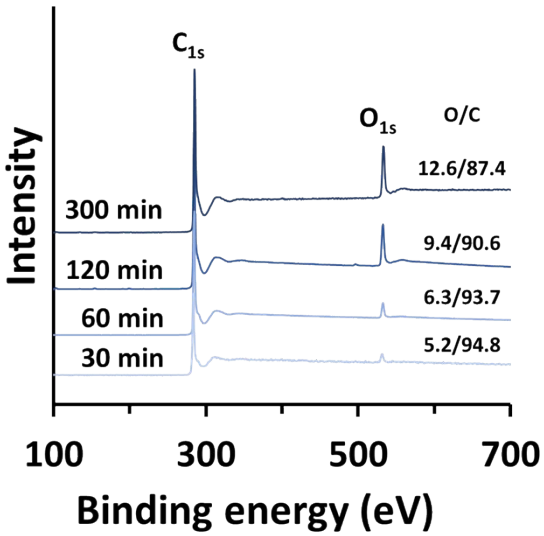

Fig. S9 Survey XPS spectra of CC after ozone irradiation to introduce oxygen functional groups to the CC surface.

SEI/CC^R can be handled in dry air for ca. 1 h with no serious degradation

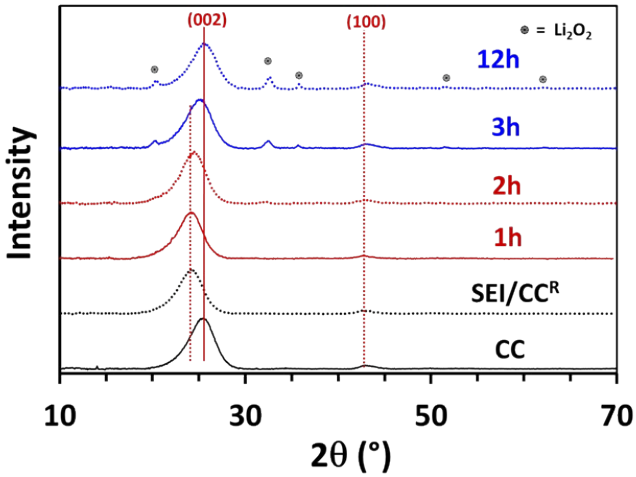

Fig. S10 Change of XRD patterns of SEI/CC^R when stored in the dry-room condition (air, dew point = -40 °C) during 1, 2, 3, and 12 h. From 2h-exposure, the d_{002} peak begins to shift to the positive 2θ direction along with the appearance of Li_2O_2.

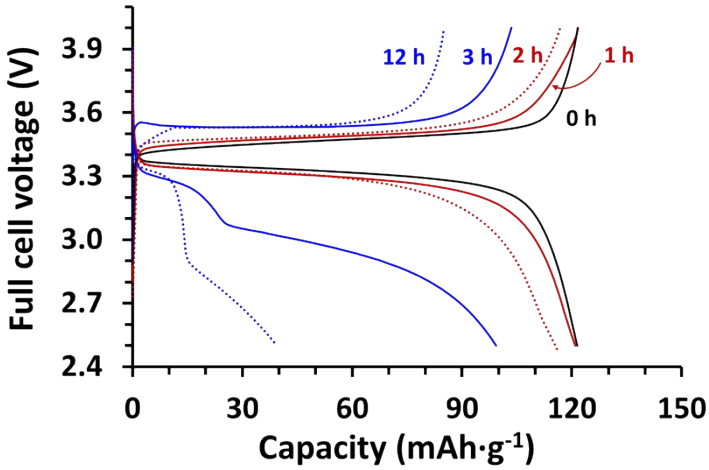

Fig. S11 C/D profiles of AFLIBs consisting of SEI/CC^R exposed to dry air and LFP at 1.0 C.